Original Article

Mechanical failure dependence on the electrical history of lead zirconate titanate thin films

K. Coleman [a,b,*,1], M. Ritter [a,c,1], R. Bermejo [b,c], S. Trolier-McKinstry [a,b]

[a] *Materials Research Institute, Pennsylvania State University, University Park, PA, United States*
[b] *Department of Materials Science and Engineering, Pennsylvania State University, University Park, PA, United States*
[c] *Department of Materials Science, Montanuniversitaet Leoben, Austria*

A B S T R A C T

Piezoelectric micromechanical systems (piezoMEMS) are often subjected to harsh mechanical and electrical loads during operation. This study evaluates the effects of the electrical history of a lead zirconate titanate (PZT) layer on the electro-mechanical response and structural limits of multilayer stacks. Electro-mechanical characterization was performed under biaxial bending employing the Ball-on-three Balls (B3B) test on virgin, poled, and DC biased (80 kV/cm) samples. No significant effect on the characteristic strength or Weibull modulus of the stack was observed. However, the crack initiation stress was highest for the virgin samples ($\sigma_0 \sim 485 \pm 30$ MPa); this decreased for both poled samples ($\sigma_0 \sim 410 \pm 30$ MPa), and samples measured under 80 kV/cm ($\sigma_0 \sim 433 \pm 30$ MPa). *in situ* ε_r and loss tangent measurements suggested electromechanical loading conditions can destabilize the domain structure. Overall, the electrical history and electromechanical loading conditions can reduce the PZT film's fracture resistance.

1. Introduction

Piezoelectric microelectromechanical systems (piezoMEMS) are used in actuators, transducers, sensors, and energy harvesting devices [1–3]. These devices are typically fabricated as stacks containing thin active piezoelectric layers (typically between 0.1–5 μm in thickness) grown on a passive elastic layer (e.g. Si) [4]. The small thickness of the piezoelectric film enables significant reduction in the voltage required to reach target electric fields, compared to bulk ceramics or single crystals. Their performance depends on the piezoelectric response of the film layer as well as the total stress/strain that the films can withstand. The main figures of merits (FoM) for these applications are related to the piezoelectric coefficient (e_{31f}) and the relative dielectric constant (ε_r) of the film; for actuators, the figure of merit is e_{31f}, for voltage-based sensors $\frac{e_{31f}}{\varepsilon_r}$, and for energy harvesters $\frac{e_{31f}^2}{\varepsilon_r}$ [5–7]. Lead zirconate titanate (PZT) with a morphotropic phase boundary composition of Pb(Zr$_{0.52}$Ti$_{0.48}$)O$_3$ is commercially used in many applications because of its high piezoelectric coefficient [1,2,8]. As suggested by FoM, the large piezoelectric coefficient leads to higher sensitivity, larger displacements, and power outputs. Tailoring the properties of the piezoelectric

thin film can enhance the device performance. In this regard, e_{31f} depends on several factors including: crystallographic orientation [9,10], stress and domain alignment [11,12], composition and microstructure control [13,14], and the degree of clamping [15,16].

In order to guarantee high performance of the stack, the structural integrity of the film must also be preserved during electromechanical service conditions. Due to the inherent brittleness of PZT [17,18], cracking of the film layers is a common problem, leading to a degradation of the electrical properties of the stack and/or complete failure [19–21]. Recent studies have shown that failure of the stack *under electrical load* begins with cracking in the PZT films [19,20,22]. Moreover, it has recently been shown that *mechanical failure* of PZT films on Si substrates may occur in two stages [20]. First, a crack initiates in the top PZT layer at a stress below the fracture strength of the stack, propagating through the film thickness and arresting at the substrate [23]. Under the same testing conditions and substrate architecture, thicker PZT films are more susceptible to cracking at a given film stress than thinner films. To model such behavior, a finite fracture mechanics approach that sets the conditions for failure of the film using a coupled stress-energy criterion has been employed [24,25]. According to this approach, thicker films build up a higher potential energy and thus can fulfill the fracture

criterion under lower applied loads [23,24]. Following this initial failure, upon increasing mechanical load further, the crack propagates through the stack, eventually causing final fracture.

Missing in the literature is work that quantifies the onset of cracking in either poled or electromechanically loaded PZT thin films. It is well known that under applied electric fields, the domain structure will change, which in turn causes reorientation of the spontaneous strain. Although this effect is more pronounced for piezoelectric ceramics [26–29], small changes in the ferroelastic domain structure have been reported in piezoelectric thin films [30,31]. Additionally, while the electric field (E) is applied, it will generate a stress (σ_e) in the film, which depends on the piezoelectric response ($e_{31,f}$) and the electrostrictive response (M) as shown in Eq. (1), where c is the material's stiffness. For PZT thin films, it is assumed that since $e_{31,f}$ is much larger than M, the electrostrictive term can be ignored.

$$\sigma_e = e_{31,f}E + McE^2 \qquad (1)$$

This work aims to understand how the electrical history and load of the piezoelectric film affects its performance by investigating property changes and mechanical limits. Dielectric and piezoelectric properties of PZT thin films with various electrical conditions (virgin, poled, and under DC bias) are measured in order to determine the figures of merit based on the electrical history. Additionally, mechanical biaxial loading is performed to determine the influence of the electrical history on the crack initiation stress and crack propagation in the PZT thin film and stack, respectively. The results are analyzed and compared with the response of similar PZT films under pure mechanical loading.

2. Materials and methods

2.1. Sample preparation and materials characterization

Niobium doped PZT ($Pb_{0.99}(Zr_{0.52}Ti_{0.48})_{0.98}Nb_{0.02}O_3$) films were grown by chemical solution deposition on a platinized 4-inch Si wafers (NOVA Electronic Materials) as described elsewhere [31,32]. A total of 20 layers (each layer thickness was ~80 nm) was deposited on the substrate, which yielded a thickness of ~1.6 μm, as measured over an etch step using a contact profilometer (KLA Tencor 16+). The stack has six layers: a 1.6 μm PZT layer, a 100 nm Pt bottom electrode, a 20 nm Ti/TiO₂ adhesion layer, 1 μm SiO₂ layer, ~500 μm Si substrate, and a 1 μm SiO₂ layer. The structure of the stack is shown in Fig. 1. The film's crystallographic orientation was determined using X-ray Diffraction (XRD) with a PANalytical Empyrean diffractometer with a Cu Kα X-Ray source. The grain size was determined using the line intercept method [33] on several micrographs, taken with a field emission scanning electron microscope (FESEM).

Pt top electrodes were deposited to a thickness of 100 nm using a Kurt Lesker CMS-18 sputter tool. The design of the top electrode (shown in Fig. 1, top right) covers the center of the sample, with a 1 mm diameter circle and a contact pad to the side. This electrode design allows for easy contact during mechanical loading and makes it possible to pole the center without damaging the surface with a probe tip, which could affect subsequent mechanical measurements.

The wafers were diced into square specimens of 12×12 mm². Specimens cut from the die were randomly classified into three samples, referred to as virgin, poled, and under DC biased. The virgin specimens did not see any electric fields prior to or during mechanical measurements, and were taken as reference material. The poled samples were heated to 150 °C and a DC bias of 13 V (~80 kV/cm) was applied using Hewlett-Packard PA-meter for 15 min. Wires were attached to the sample under DC bias using silver epoxy (Ted Pella silver conductive epoxy) to apply the electric field during the mechanical tests. The exposed part of the wires was covered with insulating epoxy to avoid a short circuit inside the testing setup.

2.2. Measurement of electrical properties

The film's relative permittivity and loss were recorded as a function of frequency (100 Hz to 100 kHz) using a Hewlett Packard 4284A precision LCR meter with a small (30 mV) AC signal applied to the bottom electrode. The polarization – electric field (P-E) hysteresis loop was measured at 100 Hz using a Radiant Precision Multiferroic Ferroelectric Tester [31]. Additionally, the Rayleigh behavior of the permittivity was measured up to 35 kV/cm (~ ½ the coercive field, E_c, at 1 kHz). The $e_{31,f}$ was measured using the wafer flexure method described by Wilke et al. [34]. All experiments were conducted under ambient conditions (~20 °C and ~40–60% RH), and a minimum of three specimens per sample type was used for each measurement.

2.3. Electromechanical loading: ball on three ball testing

The relationship between the electric fields and the structural limits of PZT thin films was tested using the ball-on-three-balls (B3B) biaxial bending test using a plate-like test setup [23,35,36]. In the B3B, the specimen (e.g. a plate or a disc) is supported by three balls on the upper side and loaded by a fourth ball on the center of the lower side (see Fig. 1, left). This leads to a well-defined biaxial stress field, with the highest tensile stresses acting in the middle of the surface, opposite to the one loading ball [35]. One advantage of this method is that the maximal stress during bending occurs in the center of the specimen, far from the edges, thus avoiding fracture due to cutting damage at the edges and/or corners of the specimen. Using the B3B set up, the characteristic stack strength of the different samples (loading to failure) and the stress required for crack initiation in the PZT layer (pre-loading and unloading for inspection) were determined. Assuming a homogenous sample, the stress corresponding to the applied load was calculated using the following equation:

$$\sigma_{max} = f\frac{F}{t^2} \, , \qquad (2)$$

where F is the applied load, t is the thickness of the sample and f is a geometrical factor, which depends on the thickness and diameter of the specimen and the radius of the balls. To give an example, for specimens with a thickness of $t \sim 0.5$ mm, with a Poisson's ratio, $\nu \sim 0.3$, a geometrical factor f of ~2.4 is obtained. More details on the B3B method can be found in [28,29].

The strength of the virgin, poled, and under DC bias samples was determined using a minimum of 10 specimens (per sample) tested following the same procedure (pre-load of about 10 N and a displacement-controlled rate of 0.1 mm/min) using a universal tester (Instron, Ma). Weibull statistics were performed according to the ASTM standards [37,38]. The strength of the Pt/Ti/TiO₂/SiO₂/Si/SiO₂ substrate was also measured for comparison. The poled samples were all aged a minimum of 20 h after poling. The samples under DC bias had 13 V (~80 kV/cm) applied during the mechanical measurements and had no exposure to an electric field prior to measurement. The DC field was applied using a Keysight E4980A precision LCR meter and the permittivity was also measured during the mechanical testing using the same LCR meter with a 30 mV 1 kHz signal superimposed on the DC bias. The strength of the stack was determined by introducing the fracture force, F_{max}, into Eq. (2). For this work, since most of the stack thickness is from the Si substrate, it is assumed σ_{max} is the stress in the Si layer. The stresses in each of the layers is calculated as described in the supplemental materials [23].

In order to determine the crack initiation stress, an additional set of five specimens of each sample with distinct electrical history was loaded
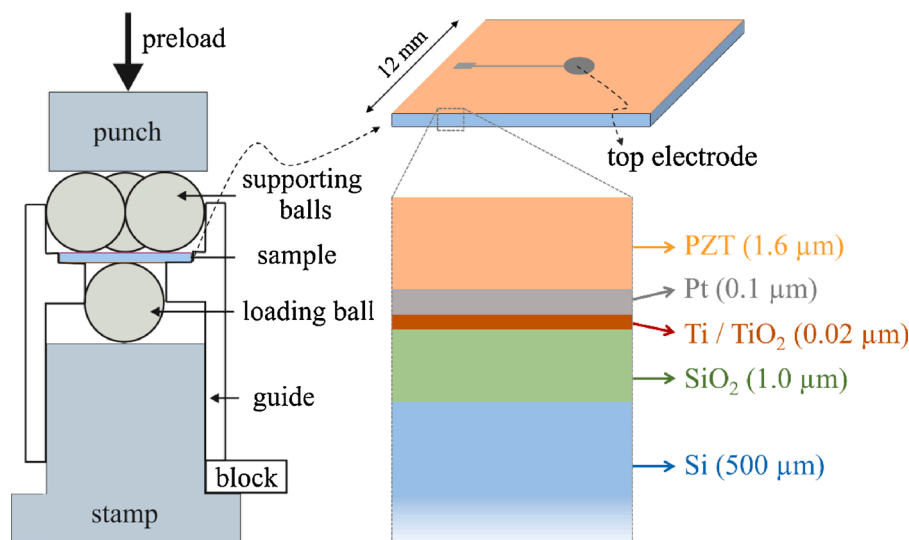
Fig. 1. The B3B setup, showing the 4 balls and the specimen in the middle, as well as the structure of the samples from the 12×12 mm^2 specimen. A Pt electrode (gray) is deposited on the PZT top surface (orange layer) to enable contact to the center of the specimen. It consists of a circle with a diameter of 1 mm in the center, a 100 μm wide trace and a 400 μm x 400 μm square close to the edge. A cross section showing each layer in the stack is also depicted (not to scale).

between 20–70 % of the corresponding characteristic strength[2] using the ball on three ball method. A similar procedure is reported in [23]. The pre-cracks initiated during the loading process were identified using an optical microscope in dark field mode. The force at which cracks were first observed was recorded as the applied force for cracking.

3. Results and discussion

3.1. Structural characterization

Fig. 2a shows the microstructure of the PZT layer, with an average lateral grain size of 126 ± 54 nm. Fig. 2b shows the cross section of the sample, in which individually deposited layers can be identified; a small amount of pyrochlore or fluorite grains is apparent at individual crystallization interfaces. The thickness of the PZT films was ~1.6 μm. Fig. 3 shows the XRD patterns corresponding to the PZT layer. The film had an approximately random orientation.

3.2. Electrical characterization

At 1 kHz under low oscillating electric fields (18.75 V/cm), ε_r was 1100 ± 24, 1073 ± 16, and 740 ± 16 for the virgin, poled, and under DC bias samples, respectively. As the frequency increased, ε_r decreased slightly for all samples. The relative permittivity was also measured as a function of increasing AC field (see supplemental materials for more details). In this low field regime, a linear Rayleigh-like regime was identified (Eq. 3):

$$\varepsilon_r = \varepsilon_{init} + \alpha E_{AC} \tag{3}$$

The irreversible Rayleigh parameter, α, captures the irreversible domain wall motion contribution and ε_{init} includes both the intrinsic and reversible domain wall contributions to the permittivity. A linear Rayleigh regime for all samples was fitted between 7 and 23 kV/cm (~10−50% E_c) with R^2 of 0.994 or higher. In the Rayleigh regime, ε_{init} was 1099 ± 17, 1059 ± 17, 735 ± 17 for the virgin, poled, and film under DC bias, respectively. α was 22 ± 2, 15.75 ± 1.25, 5.5 ± 0.14 cm/kV for the virgin, poled, and film under DC bias, respectively.

The low ε_{init} for the sample under DC bias is due to dielectric stiffening. The difference between ε_{init} for the virgin and poled sample was modest, suggesting that there is a limited ferroelastic reorientation with an applied field. As expected, the sample under DC bias has the lowest α_{ray}, which is due to the stabilization of the domain structure and intrinsic dielectric tunability [39]. The observation that $\alpha_{ray,virgin} > \alpha_{ray,poled}$ is believed to be due to the removal of domain walls as a result of poling the sample.

The polarization versus electric field hysteresis loops indicate some differences between the samples (see the supplemental materials Fig. SI.2). The positive remanent polarization (P_r) was 16.7 μC/cm^2, 18.5 μC/cm^2, 17.7 μC/cm^2 for the virgin, poled, and under DC bias film, respectively. The virgin film's negative P_r was -19.2 μC/cm^2 and this slight imprint was removed by applying an electric field as shown by the symmetric loop for the poled and under DC bias films.

The changes in α, P_r, and E_c suggests changes in the domain structure and domain alignment. A schematic illustration of possible domain structures for the different samples is given in the supplemental materials. As indicated by the largest P_r, the poled sample should have more domains aligned with the applied electric field compared to the virgin sample. The sample under DC bias is also expected to have more domains aligned and less domain walls than the virgin sample. However, this alignment is incomplete since the film under DC bias is only under electric field during the measurement.

Due to the differences in domain structure, the films should have different piezoelectric coefficients and FoM. The various FoM are shown in Table SI.1, where the piezoelectric coefficient, $e_{31,f}$, was measured to be 0 C/m^2, -6.5 C/m^2 and -4.1 C/m^2 for the virgin, poled, and under DC bias sample, respectively. The poled sample has the largest coefficient, presumably because the sample under DC bias was only partially poled. The poled sample also had the highest FoM for all applications compared to the virgin and the sample under a DC bias. An additional sample that was poled, aged for 24 h, and then measured under a DC bias is also reported in Table SI.1. The piezoelectric coefficient was slightly lower than the poled sample due to aging, and the permittivity was also lower because of the DC bias. As a result, it had the largest FoM for sensors and energy harvesters.

3.3. Strength distributions and fracture analyses

Fig. 4 shows the probability of failure, P_f, versus the failure stress, σ_f,
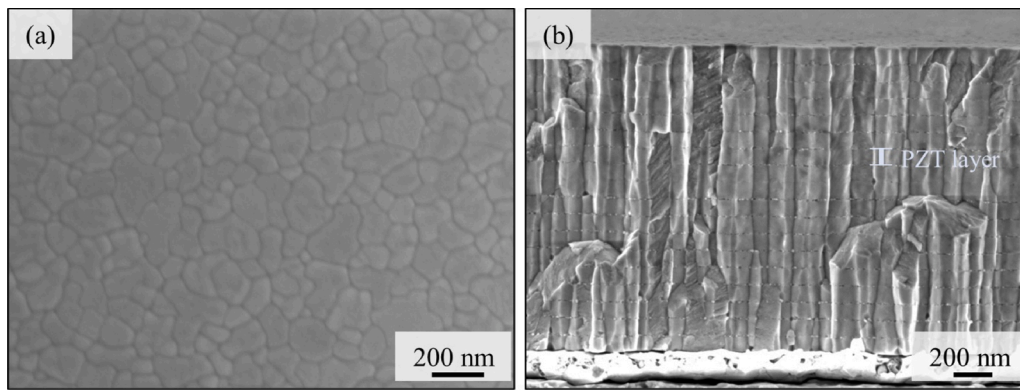
---

[2] The characteristic strength is the applied stress that corresponds to a probability of failure of ~63%, according to Weibull analysis.

Fig. 2. (*a*) Top view SEM image showing the grain size of the PZT layer. (*b*) Cross sectional SEM image showing the layered structure of the 1.6 µm thick PZT layer, as well as the platinum bottom electrode.
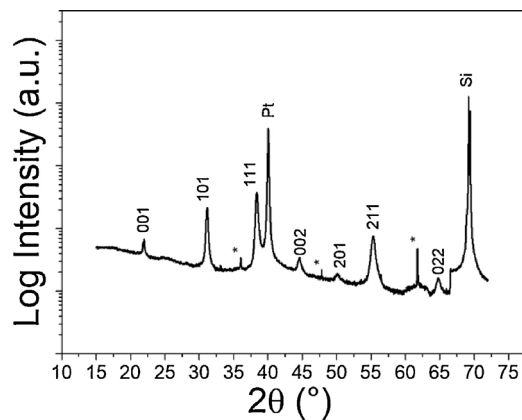

Fig. 3. XRD pattern of the PZT layer, showing random orientation. The symbol "*" indicates background peaks from the substrate.
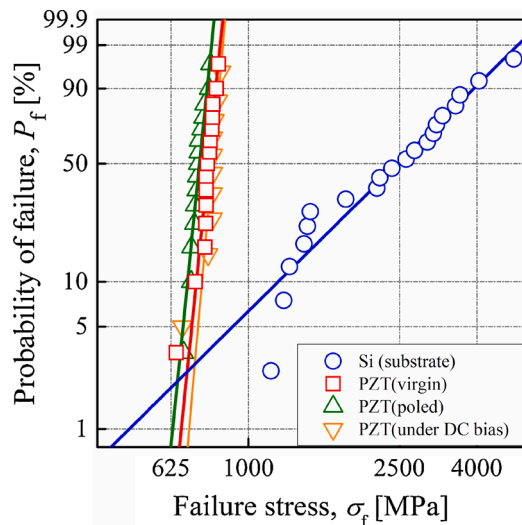

Fig. 4. Probability of failure versus failure stress in a Weibull diagram for the three samples (virgin (red square), poled (green upward triangle), and under DC bias (orange downward triangle)) and the Pt/Si sample (blue circles), as a reference. (For interpretation of the references to colour in this figure legend, the reader is referred to the web version of this article).

in a Weibull diagram for the virgin, poled, and under DC bias samples, as well as for the Pt/Si substrate (taken as a reference). The Weibull parameters (i.e. characteristic strength, σ_0, and Weibull modulus, m) were

calculated according to the ENV-845 standards [40] and are given in Table 1, along with the 90 % confidence intervals. The Weibull modulus ranged between $m = 26$ and $m = 30$ for the virgin, poled, and under DC bias sample, whereas the Pt/Si substrate's modulus was as low as $m{\sim}3$. There was no significant difference in the characteristic stack strength between virgin, poled, and under DC bias samples.

At lower loads, cracks were visible on the surface of the PZT film; this initial crack did not propagate through the entire stack. A focused ion beam etch was used to determine the initial crack length, as shown in Fig. 5. The crack propagated through the PZT layer, and stopped at the Pt layer. Pt, being metallic, may prevent crack propagation through plastic deformation. Thus, as reported previously [23], cracking occurs first in the PZT layer, followed by crack propagation through the subsequent layers. The initial crack in the PZT layer acts as the critical flaw for the failure of the remaining layers in the stack. This yields higher Weibull moduli of the PZT stacks as compared to the Si substrate, as reported elsewhere (see [23] for more details).

The stress to initiate a crack in the PZT layer depended on the electrical history as shown in Table 2. The virgin sample had cracks initiating at stresses around 500 MPa, which falls within a predicted crack initiation range reported for PZT films with similar thicknesses [19,23]. However, crack initiation occurred at lower stresses for both the poled sample, and the sample measured under DC bias (around 400 MPa). Initially this difference was attributed to inaccuracies in the calculated piezoelectric stress. It was assumed that the $e_{31,f}$ did not change with applied mechanical load or time, but other reports suggest that the piezoelectric coefficient will change with both field and stress [31,41]. However, this does not account for the decrease in crack initiation stress for the poled sample, since it was not under an applied electric field during B3B loading and there is a statistically significant decrease in the crack initiation stress compared to the virgin sample.

There are a few hypotheses for the observed reduction in the film's crack initiation stress with applied fields. First, there may be some

Table 1
Weibull modulus, m, characteristic strength, σ_0, and applied force and stress for cracking for the different samples. Values in [] represent the 90 % confidence interval.

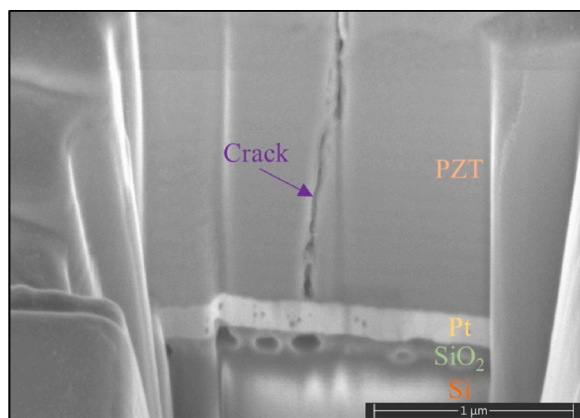| Sample state	Weibull modulus m [–]	Characteristic strength σ_0 [MPa]
Virgin	26 [17–34]	795 [780–811]
Poled	26 [17–34]	754 [739–769]
Under DC bias	30 [16–40]	815 [797–833]
Si	2.6 [1.8–3.3]	2851 [2428–3356]

Fig. 5. FIB image showing the crack stop at the interface of the PZT and Pt seed layer beneath. The image was prepared using a FEI Scios Focused Ion Beam (FIB) system. The porosity in the SiO_2 layer may be due to lead diffusion through the stack, and some damage from the FIB.

Table 2
Calculated stresses (applied, piezoelectric, and residual stresses) in the PZT films and total stress for crack initiation for each film based on its electric history. There is an additional systematic error of the residual stress calculation for the wafer of $\pm$ 30 MPa.

Sample	Force Cracking observed [N]	Applied Stress in the PZT layer [MPa]	Residual Stresses [MPa]	Piezoelectric Stress [MPa]	Total Stress for Crack Initiation [MPa]
Virgin	49 ± 3.8[δ]	335 ± 26	150	0	485 ± 26
Poled	37.5 ± 3.8	260 ± 26	150	0	410 ± 26
Under DC bias	35.2 ± 3.8	240 ± 26	150	33 ± 3	430 ± 29

[δ] The error corresponds to the interval of applied forces between no-cracking and cracking observation on each sample.

differences in the domain wall motion between the films. The irreversible Rayleigh coefficient was largest for the virgin sample. Non-180° domain wall motion and ferroelastic domain reorientation have been shown to enhance the fracture resistance [26,29]. If domains are unable to reorient to reduce the applied stress, then PZT would have a lower apparent fracture toughness. However, the reduction in the irreversible Rayleigh coefficient may be due to the large reduction in the number of 180° domain walls, and it is inconclusive whether the amount of ferroelastic domain reorientation is also changed during mechanical loading. Alternatively, the generation of local strain during the poling process is also proposed to cause this reduction in crack initiation stress. Under an applied electric field, domains align to the polarization direction, and previous reports suggest limited ferroelastic reorientation occurs in clamped films [16]. Ferroelastic domain reorientation will create localized stresses, and may result in the lower fracture resistance in the poled sample. Both the poled sample and the film under DC bias may experience some ferroelastic domain reorientation. However, it is anticipated that the poled film may have more domain alignment and may also have slightly more local strains from ferroelastic switching. The extent of ferroelastic domain reorientation is not measured in this study and therefore future work should explore the mechanism governing this trend. Overall, this study suggests that poling and electric fields can reduce the crack initiation stress by up to 15 %.

3.4. In situ property measurements under electromechanical loads

To further explore the relationship between electromechanical

loading and the changes in the properties, a total of three PZT films under DC bias had their relative permittivity and loss tangent recorded during the B3B loading experiment (Fig. 6). The plots are segmented into three regions (I, II, and III). Region I is the preload region, where the PZT sample is loaded up to 10 N prior to the start of the experiment. Region II begins when the DC bias of 80 kV/cm is applied, the permittivity is recorded, and the tensile stress is applied in the PZT layer. During this stage, cracks were not observed on the film's surface, since the stresses were lower than the reported crack initiation stress. Region III corresponds to the forces at which surface cracks were observed.

In this electromechanical loading condition, the electric field is out-of-plane, which would favor out-of-plane polarization. However, the mechanical loading would favor more in-plane domains. It is suggested that competition between these two loads on the film may destabilize the domain structure. This would account for the initial increase in the relative permittivity and loss tangent for Region II. There is a clear peak in the relative permittivity at a downward force of around 20 N, which corresponds to an applied tensile stress of 137 MPa. Around 20 N in Region II, the permittivity begins to decrease and this continues in Region III, where cracks are formed on the surface. The decrease in the calculated value of permittivity may be due a variety of factors. There may be a reduction in domain wall motion at a certain stress level. This decrease could also be related to the formation of internal cracks, where air would act as a parasitic capacitor layer, reducing the overall capacitance. Alternatively, the effective electrode area may decrease due to delamination, such that the calculated permittivity is underestimated. Lastly, the PZT film may be locally de-clamped as the crack forms, such that domains can align with the electric field out-of-plane. This would lower the overall relative permittivity. A recent study investigating PZT ceramics also showed a peak in the relative permittivity as a function of applied stress [42]. While that study focused on compressive stress and no cracking was reported [42], there was a clear peak in the relative permittivity. That study suggests competing mechanisms between domain reorientation and domain pinning (e.g. sample de-aging) may have cause the peak near their reported coercive stress value.

To further investigate the effects of mechanical loads on the destabilization of the domain structure, the aging rate of the permittivity was determined after removing the mechanical preload (10 N) on virgin and poled films. It is well known that mechanical stresses can be used to stabilize or destabilize the domain structure and polarization for PZT ceramics [43,44] depending on the orientation of the stress relative to the polarization. However, this is less explored in PZT thin films and the aging rate upon removal of stress is not well reported. Fig. 7 shows the normalized change in the permittivity as a function of time after removal of the pre-load. A linear fit of the permittivity suggests an aging rate of ~1.2 % per decade for both poled and virgin samples. This is in good agreement with the dielectric aging rates recorded after removal of an electric field [45], suggesting the rate at which the global domain structure approaches equilibrium is independent of a mechanical or electrical load.

4. Conclusions

The electric history of the sample dictates the performance of the films, influences the FoM, and may reduce the crack initiation stress. While poling enhances the piezoelectric response of the film, it reduces the stress that the films can withstand during operation, prior to cracking. The crack initiation stress was reduced by roughly 15 % under these conditions compared to the virgin film. The reduction in crack initiation stress may be due to the creation of local stress or reduction in domain wall motion. Lastly, the application of electromechanical loads may destabilize the domain structure and the removal of mechanical loads leads to similar dielectric aging rates that are reported after the removal of electrical loads. This suggests that the time for the domain structure to reach a new equilibrium position is independent of the type
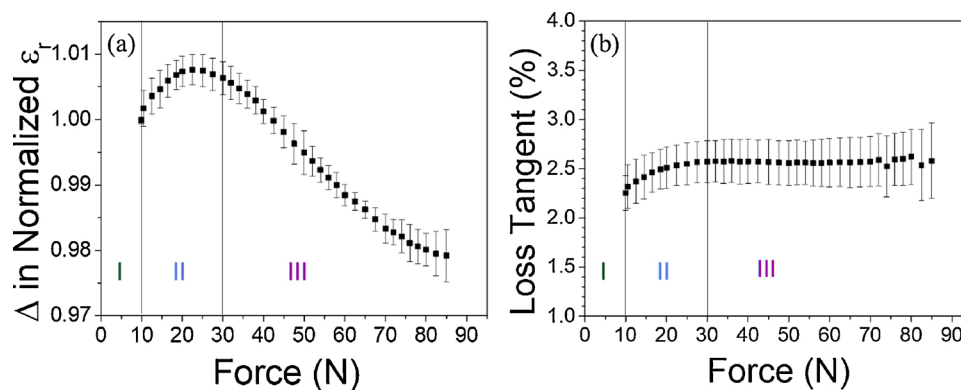
Fig. 6. Change in normalized relative permittivity (a) and change in loss tangent (b) as a function of the load force during the B3B measurements. The three regions can be allocated to three different conditions, governing the electrical properties of the PZT layer. Region *I* is the preload region. Region *II* is the regions before cracks are observed and Regions *III* is the regions after cracks were observed on the surface.
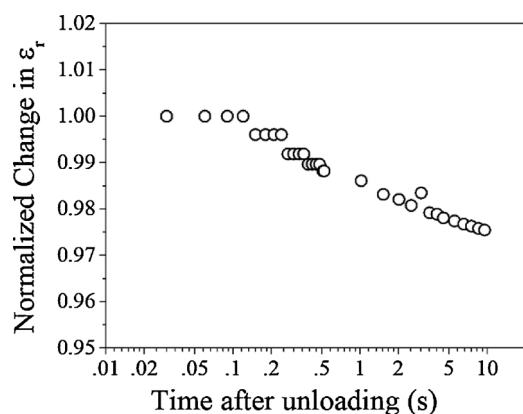

Fig. 7. Normalized change in the relative permittivity as a function of time (log) to determine the aging rate after the removal of a mechanical load. The dielectric aging rate was ~1.2 % per decade.

of load. This study emphasizes the necessity to quantify the mechanical loads on piezoelectric films, as they may destabilize the domain structure. In addition, failure may ensue at lower loads than predicted from mechanical-only testing in electromechanical applications.

Declaration of Competing Interest

The authors report no declarations of interest.

Acknowledgements

Appendix A. Supplementary data

Supplementary material related to this article can be found, in the online version, at doi:https://doi.org/10.1016/j.jeurceramsoc.2020.11.002.

References

[1] N. Izyumskaya, Y.I. Alivov, S.J. Cho, H. Morkoç, H. Lee, Y.S. Kang, Processing, structure, properties, and applications of PZT thin films, Crit. Rev. Solid State Mater. Sci. 32 (2007) 111–202, https://doi.org/10.1080/10408430701707347.

[2] P. Muralt, R.G. Polcawich, S. Trolier-McKinstry, Piezoelectric thin films for sensors, actuators, and energy harvesting, MRS Bull. 34 (2009) 658–664, https://doi.org/10.1557/mrs2009.177.

[3] S.G. Kim, S. Priya, I. Kanno, Piezoelectric MEMS for energy harvesting, MRS Bull. 37 (2012) 1039–1050, https://doi.org/10.1557/mrs.2012.275.

[4] C.B. Eom, S. Trolier-McKinstry, Thin-film piezoelectric MEMS, MRS Bull. 37 (2012) 1007–1017, https://doi.org/10.1557/mrs.2012.273.

[5] J.F. Tressler, S. Alkoy, R.E. Newnham, Piezoelectric sensors and sensor materials, J. Electroceram. 2 (1998) 257–272, https://doi.org/10.1023/A:1009926623551.

[6] S. Tadigadapa, K. Mateti, Piezoelectric MEMS sensors: state-of-the-art and perspectives, Meas. Sci. Technol. 20 (2009), https://doi.org/10.1088/0957-0233/20/9/092001.

[7] C.A. Randall, A. Kelnberger, G.Y. Yang, R.E. Eitel, T.R. Shrout, High strain piezoelectric multilayer actuators - A material science and engineering challenge, J. Electroceram. 14 (2005) 177–191, https://doi.org/10.1007/s10832-005-0956-5.

[8] D. Damjanovic, Ferroelectric, dielectric and piezoelectric properties of ferroelectric thin films and ceramics, Rep. Prog. Phys. 61 (1998) 1267–1324, https://doi.org/10.1088/0034-4885/61/9/002.

[9] J. Ouyang, R. Ramesh, A.L. Roytburd, Intrinsic effective piezoelectric coefficient e31,f for ferroelectric thin films, Appl. Phys. Lett. 86 (2005) 152901, https://doi.org/10.1063/1.1899252.

[10] S. Yokoyama, Y. Honda, H. Morioka, S. Okamoto, H. Funakubo, T. Iijima, H. Matsuda, K. Saito, T. Yamamoto, H. Okino, O. Sakata, S. Kimura, Dependence of electrical properties of epitaxial thick films on crystal orientation and ratio, J. Appl. Phys. 98 (2006), 094106, https://doi.org/10.1063/1.2126156.

[11] M.A. Dubois, P. Muralt, Measurement of the effective transverse piezoelectric coefficient e31,f of AlN and Pb(Zrx,Ti1-x)O3 thin films, Sens. Actuators A Phys. 77 (1999) 106–112, https://doi.org/10.1016/S0924-4247(99)00070-9.

[12] B.A. Tuttle, J.A. Voigt, T.J. Garino, D.C. Goodnow, R.W. Schwartz, D.L. Lamppa, T.J. Headley, M.O. Eatough, Chemically prepared Pb(Zr, Ti)O3 thin films: the effects of orientation and stress, ISAF' 92 Proc. Eighth IEEE Int. Symp. Appl. Ferroelectr. (1992) 344–348, https://doi.org/10.1109/ISAF.1992.300703.

[13] M. Eatough, D. Dimos, B.A. Tuttle, W.L. Warren, R. Bank, A study of switching behavior in Pb (Zr, Ti)O3 thin films using X-Ray diffraction, Mater. Res. Soc. Symp. Proc. 361 (1995) 111–116. http://journals.cambridge.org/abstract_S0883769400003614.

[14] K. Tomioka, F. Kurokawa, R. Yokokawa, H. Kotera, K. Adachi, I. Kanno, Composition dependence of piezoelectric properties of Pb(Zr,Ti) O3 films prepared by combinatorial sputtering, J. Appl. Phys. 57 (2012) 09LA12, https://doi.org/10.1143/JJAP.51.09LA12.

[15] G. Han, J. Ryu, W.H. Yoon, J.J. Choi, B.D. Hahn, D.S. Park, Effect of film thickness on the piezoelectric properties of lead zirconate titanate thick films fabricated by aerosol deposition, J. Am. Ceram. Soc. 94 (2011) 1509–1513, https://doi.org/10.1111/j.1551-2916.2010.04276.x.

[16] M. Wallace, R.L. Johnson-Wilke, G. Esteves, C.M. Fancher, R.H.T. Wilke, J.L. Jones, S. Trolier-McKinstry, In situ measurement of increased ferroelectric/ferroelastic domain wall motion in declamped tetragonal lead zirconate titanate thin films, J. Appl. Phys. 117 (2015), 054103, https://doi.org/10.1063/1.4907394.

[17] S.L. dos Santos e Lucato, D.C. Lupascu, J. Rödel, Effect of poling direction on R-curve behavior in lead zirconate titanate, J. Am. Ceram. Soc. 83 (2000) 424–426, https://doi.org/10.1111/j.1151-2916.2000.tb01210.x.

[18] I. Westram, D. Lupascu, J. Rödel, Electric-field-Induced crack initiation from a notch in a ferroelectric ceramic, J. Am. Ceram. Soc. 90 (2007) 2849–2854, https://doi.org/10.1111/j.1551-2916.2007.01737.x.

[19] A. Mazzalai, D. Balma, N. Chidambaram, P. Muralt, L. Colombo, T. Schmitz-Kempen, Dynamic and long-time tests of the transverse piezoelectric coefficient in PZT thin films, IEEE Int. Symp. Appl. Ferroelectr. Proc. (2014) 1–4, https://doi.org/10.1109/ISAF.2014.6922998.

[20] W. Zhu, T. Borman, K. Decesaris, B. Truong, M.M. Lieu, S.W. Ko, P. Mardilovich, S. Trolier-McKinstry, Influence of PbO content on the dielectric failure of Nb -

doped {100} - oriented lead zirconate titanate films, J. Am. Ceram. Soc. 102 (2018) 1734–1740, https://doi.org/10.1111/jace.16000.

[21] H.D. Chen, K.R. Udayakumar, K.K. Li, C.J. Gaskey, L.E. Cross, Dielectric breakdown strength in sol-gel derived PZT thick films, Integr. Ferroelectr. 15 (1997) 89–98, https://doi.org/10.1080/10584589708015699.

[22] A. Furuta, K. Uchino, Dynamic observation of crack propagation in piezoelectric multilayer actuators, J. Am. Ceram. Soc. 76 (1993) 1615–1617, https://doi.org/10.1111/j.1151-2916.1993.tb03950.x.

[23] K. Coleman, R. Bermejo, D. Leguillon, S. Trolier-McKinstry, Thickness dependence of crack initiation and propagation in piezoelectric microelectromechanical stacks, Acta Mater. 191 (2020) 245–252, https://doi.org/10.1016/j.actamat.2020.03.030.

[24] D. Leguillon, Strength or toughness? A criterion for crack onset at a notch, Eur. J. Mech. A Solids 21 (2002) 61–72, https://doi.org/10.1016/S0997-7538(01)01184-6.

[25] D. Leguillon, J. Li, E. Martin, Multi-cracking in brittle thin layers and coatings using a FFM model, Eur. J. Mech. A Solids 63 (2017) 14–21, https://doi.org/10.1016/j.euromechsol.2016.12.003.

[26] Y.H. Seo, A. Benčan, J. Koruza, B. Malič, M. Kosec, K.G. Webber, Compositional dependence of R-curve behavior in soft Pb(Zr$_{1-x}$Ti$_x$)O$_3$ ceramics, J. Am. Ceram. Soc. 94 (2011) 4419–4425, https://doi.org/10.1111/j.1551-2916.2011.04889.x.

[27] K. Mehta, A.V. Virkar, Fracture mechanisms in ferroelectric-ferroelastic lead zirconate titanate (Zr: Ti=0.54:0.46) ceramics, J. Am. Ceram. Soc. 73 (1990) 567–574, https://doi.org/10.1111/j.1151-2916.1990.tb06554.x.

[28] J.M. Calderon-Moreno, M. Popa, Fracture toughness anisotropy by indentation and SEVNB on tetragonal PZT polycrystals, Mater. Sci. Eng. A319-321 (2001) 692–696, https://doi.org/10.1016/S0921-5093(00)02020-7.

[29] R. Bermejo, H. Grünbichler, J. Kreith, C. Auer, Fracture resistance of a doped PZT ceramic for multilayer piezoelectric actuators: effect of mechanical load and temperature, J. Eur. Ceram. Soc. 30 (2010) 705–712, https://doi.org/10.1016/j.jeurceramsoc.2009.08.013.

[30] R.J. Zednik, A. Varatharajan, M. Oliver, N. Valanoor, P.C. McIntyre, Mobile ferroelastic domain walls in nanocrystalline PZT films: the direct piezoelectric effect, Adv. Funct. Mater. 21 (2011) 3104–3110, https://doi.org/10.1002/adfm.201100445.

[31] K. Coleman, J. Walker, T. Beechem, S. Trolier-McKinstry, Effects of stresses on the dielectric and piezoelectric properties of Pb(Zr$_{0.52}$Ti$_{0.48}$)O$_3$ thin films, J. Appl. Phys. 126 (2019) 034101, https://doi.org/10.1063/1.5095765.

[32] D.G. Wang, C.Z. Chen, J. Ma, T.H. Liu, Lead-based titanate ferroelectric thin films fabricated by a sol-gel technique, Appl. Surf. Sci. 255 (2008) 1637–1645, https://doi.org/10.1016/j.apsusc.2008.09.053.

[33] EN 623-3: "200x Advanced technical ceramics – Monolithic ceramics – General and textural properties - Part 3 : Determination of Grain Size and Size Distribution (Characterized by the Linear Intercept Method)," (n.d.) 1–21.

[34] R.H.T. Wilke, P.J. Moses, P. Jousse, C. Yeager, S. Trolier-McKinstry, Wafer mapping of the transverse piezoelectric coefficient, e$_{31,f}$, using the wafer flexure technique with sputter deposited Pt strain gauges, Sens. Actuators A Phys. 173 (2012) 152–157, https://doi.org/10.1016/j.sna.2011.10.030.

[35] A. Börger, P. Supancic, R. Danzer, The ball on three balls test for strength testing of brittle discs: stress distribution in the disc, J. Eur. Ceram. Soc. 22 (2002) 1425–1436, https://doi.org/10.1016/S0955-2219(01)00458-7.

[36] R. Danzer, P. Supancic, W. Harrer, Biaxial tensile strength test for brittle rectangular plates, J. Ceram. Soc. Japan. 114 (2006) 1054–1060, https://doi.org/10.2109/jcersj.114.1054.

[37] W. Weibull, A Statistical Theory of Strength of Materials, Royal Swedish Institute for Engineering Research, 1939.

[38] ASTM C1239-13(2018), Standard practice for reporting uniaxial strength data and estimating Weibull distribution parameters for advanced ceramics, ASTM International, West Conshohocken, PA, 2018, n.d.

[39] N. Bassiri-Gharb, I. Fujii, E. Hong, S. Trolier-McKinstry, D.V. Taylor, D. Damjanovic, Domain wall contributions to the properties of piezoelectric thin films, J. Electroceram. 19 (2007) 47–65, https://doi.org/10.1007/s10832-007-9001-1.

[40] EN 843-845, "Advanced technical ceramics - Mechanical properties of monolithic ceramics at room temperature - Part 5: Statistical analysis," 1996, (n.d.).

[41] Z. Qiu, J.S. Pulskamp, X. Lin, C. Rhee, T. Wang, R.G. Polcawich, K. Oldham, Large displacement vertical translational actuator based on piezoelectric thin films, J. Micromech. Microeng. 20 (2010), 075016, https://doi.org/10.1088/0960-1317/20/7/075016.

[42] F.H. Schader, D. Isaia, M. Weber, E. Aulbach, K.G. Webber, High-temperature stress-dependent piezoelectric and dielectric coefficient of soft Pb (Zr, Ti) O 3, J. Mater. Sci. 53 (2018) 3296–3308, https://doi.org/10.1007/s10853-017-1817-8.

[43] C. Lynch, On the development of multiaxial phenomenological constitutive laws for ferroelectric ceramics, J. Intell. Mater. Syst. Struct. 9 (1998) 555–563.

[44] T. Gransow, A. Kounga, E. Aulbach, J. Rodel, Electromechanical poling of piezoelectrics, Appl. Phys. Lett. 88 (2006), 252907, https://doi.org/10.1063/1.2216028.

[45] R.G. Polcawich, S. Trolier-McKinstry, Piezoelectric and dielectric reliability of lead zirconate titanate thin films, J. Mater. Res. 15 (2000) 2505–2513, https://doi.org/10.1557/JMR.2000.0360.